Microstructure, Microsegregation, and Mechanical Properties of Directional Solidified Mg–3.0Nd–1.5Gd Alloy

Shaojun Liu · Guangyu Yang · Wanqi Jie

Abstract The microstructure, microsegregation, and mechanical properties of directional solidified Mg–3.0Nd–1.5Gd ternary alloys were experimentally studied. Experimental results showed that the solidification microstructure was composed of dendrite primary α(Mg) phase and interdendritic α(Mg) + Mg_{12}(Nd, Gd) eutectic and Mg_5Gd phase. The primary dendrite arm spacing λ_1 and secondary dendrite arm spacing λ_2 were found to be depended on the cooling rate R in the form $\lambda_1 = 8.0415 \times 10^{-6} R^{-0.279}$ and $\lambda_2 = 6.8883 \times 10^{-6} R^{-0.205}$, respectively, under the constant temperature gradient of 40 K/mm and in the region of cooling rates from 0.4 to 4 K/s. The concentration profiles of Nd and Gd elements calculated by Scheil model were found to be deviated from the ones measured by EPMA to varying degrees, due to ignorance of the back diffusion of the solutes Nd and Gd within α(Mg) matrix. And microsegregation of Gd depended more on the growth rate, compared with Nd microsegregation. The directionally solidified experimental alloy exhibited higher strength than the non-directionally solidified alloy, and the tensile strength of the directionally solidified experimental alloy was improved, while the corresponding elongation decreased with the increase of growth rate.

KEY WORDS: Mg–Nd–Gd ternary magnesium alloy; Directional solidification microstructures; Dendrite growth; Microsegregation; Mechanical property

1 Introduction

Solidification behavior can be scientifically studied via directional solidification with the liquid quenching technology, since combination of the temperature gradient G generated by the directional solidification furnace and a constant growth rate v provides a well-defined microstructure [1]. This technology has been used for different alloys, such as aluminum alloy, nickel-based superalloy, and a few works of magnesium alloys [2–4]. Zhang et al. [2] and Zheng et al. [3] studied the morphology and microsegregation of directional solidified Mg–4Al and AX44 (Mg–4Al–4Ca, wt%) alloys, and they found that the relationship between the primary dendritic arm spacing λ_1 and growth rate v can be described by the Hunt–Lu model. Mirkovic et al. [4] analyzed the microsegregation of AZ31 and AM50 castings produced by directional solidification, and qualitative agreement but quantitative discrepancy between the experimental results and the calculated solute profiles by Scheil model was observed. However, they all mainly focus on Mg–Al-based alloys in the above researches.

In recent years, tremendous attentions have been given to Mg-RE alloys due to their high specific strength both at room temperature and elevated temperature, as well as their excellent creep resistance [5, 6]. Among them, Mg–Nd–Gd system is one of the promising materials exhibiting high creep resistance properties [7]. There have been extensive researches on the microstructure and the

S. Liu · G. Yang (✉) · W. Jie
State Key Laboratory of Solidification Processing, Northwestern Polytechnical University, Xi'an 710072, China
e-mail: ygy@nwpu.edu.cn

mechanical properties of Mg–Nd–Gd alloys in recent publications [8–10]. Negishi et al. [8] found that Mg–3Gd–3Nd alloy showed remarkable age hardening response even at 250 °C due to the formation of β'' phase with $D0_{19}$ crystalline structure, which reduced the creep rate and enhanced the creep resistance. The outstanding creep resistant property of sand-cast Mg–2.8Nd–0.3Gd–0.8Zn–0.5Zr alloy at 240 °C was associated with fine grain size [9]. Li et al. [10] studied sand-cast Mg–3.0Nd–1.5Gd–0.25Zn–0.5Zr alloy and found that the experimental alloy exhibited higher elevated temperature mechanical properties than ZM6 alloy (Mg–2.0–2.8Nd–0.2–0.7Zn–0.4–1.0Zr). Obviously, Mg–Nd–Gd-based alloy is an ideal candidate for high-temperature applications. However, there is few works reported on the solidification of Mg–Nd–Gd alloys under different casting conditions.

In order to explore solidification behavior of Mg–Nd–Gd magnesium alloy, an Mg–3.0Nd–1.5Gd ternary magnesium alloy was designed, and its microstructures, microsegregation behavior, and mechanical properties under different cooling rates have been studied based on directional solidification technique.

2 Experimental

2.1 Alloy Preparation

The experimental alloy was melt with pure Mg (99.98), pure Nd (99.9), and Mg–28%Gd master alloy in an electrical-resistance furnace under the protection of anti-oxidizing flux. The nominal composition of the experimental alloy is Nd 2.0–4.0, Gd 0.5–2.5, and balance of Mg in weight percent. The melt was held at 800 °C for 30 min, and then cooled to 760 °C and finally poured into an iron mold preheated at 250 °C with the size of Φ10 mm × 150 mm. The cast ingots were further processed into the samples of Φ7.8 mm × 90 mm for directional solidification. The real composition was measured by the inductively coupled plasma-optical emission spectrometry (ICP-OES) to be Mg–2.49Nd–1.82Gd in weight percent.

2.2 Directional Solidification Experiments

The direction solidification was undertaken in a high-temperature gradient Bridgman-type directional solidification furnace with a graphite heater and quenching system of water-cooled Ga–In–Sn liquid metals. The schematic of the furnace is shown in Fig. 1a. A special crucible was designed to prevent the oxidation of the alloy, as shown in Fig. 1b. The prepared sample (Φ7.8 mm × 90 mm) was loaded in a stainless tube crucible with 10 mm outer

diameter, 8 mm inner diameter, 120 mm in length, and sealed bottom. A thin stainless steel tube with 6 mm inner diameter, 8 mm outer diameter, and 40 mm length, named sulfur dioxide (SO_2) generator, was inserted into the top of the crucible for the alloy protection. An appropriate amount of sulfur was advanced into the generator, which was burnt at 270 °C and consume the oxygen in the crucible by forming SO_2 to keep the alloy under the protective atmosphere of SO_2.

The crucible was put in vacuum furnace with the graphite heater, pumped down to 1 Pa, backfilled with high-purity Ar gas, and then heated to 850 °C for 30 min. When the axial temperature gradient reached 40 K/mm, the sample was directionally solidified by moving the crucible downward at a given speed (10–100 μm/s) for about 40 mm, and then quenched in Ga–In–Sn liquid metals. In the analysis, the withdrawal rate was approximately used as growth rate.

The solidified samples were cut along both the longitudinal and transversal sections to investigate the quenched interface morphology, and the solidification microstructure was observed with Olympus PM-G3 type optical microscope (OM), JEOL JSM-5800 type scanning electron microscope (SEM), and Technai 30F type transmission electron microscope (TEM). The transversal sections of the completely solidified samples before etching were analyzed with EPMA-1720 in an area-scan method to examine the microsegregation, in which 100 points within an area of 200 μm × 200 μm were measured automatically. After collecting the data, a mathematical treatment was applied to obtain the concentration profiles of the alloying elements Nd and Gd. The normalized fractions were used for plotting the profiles of solute distribution. The phase analysis was conducted in an Oxford Inca type X-ray energy dispersive spectroscope (EDS). The X-ray diffraction (XRD) was performed on a X'Pert PRo MPD type instrument in the diffraction angle (2θ) range between 20° and 90°, using CuK_{α} ($\lambda = 0.154$ nm) as radiation source. The volume fraction of the second phase was measured by Image-Pro Plus 6.0 (Media Cybernetics, Inc., Bethesda, MD). The room temperature tensile properties were tested in a Zwick 150 type universal tensile testing machine with a maximum load of 150 kN and a strain rate of 1 mm/min. The test specimens were rectangular shape with 20 mm in length, 5 mm in width, and 2 mm in height, as shown in Fig. 2.

### 2.3 Determination of Dendrite Parameters

The primary dendrite arm spacing λ_1, as shown in Fig. 3, was measured in 5–7 selected regions in longitudinal sections of the solidified alloy, and the average values were calculated. The secondary dendrite arm spacing λ_2 was also measured by counting the number of secondary dendrite arms n within the length L, and get $\lambda_2 = L/(n-1)$. Each
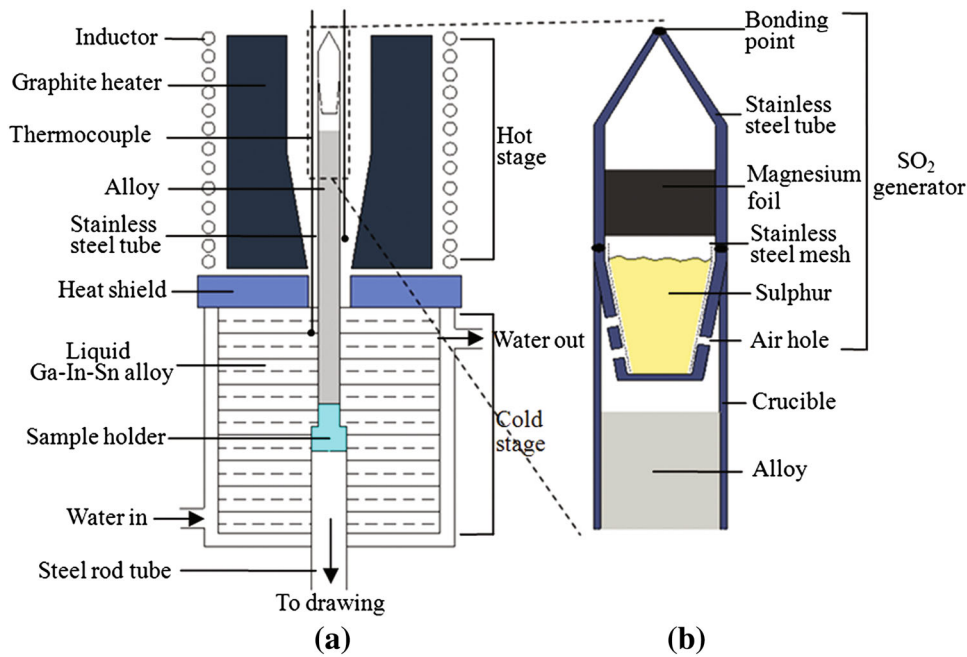
Fig. 1 The Bridgman-type directional solidification furnace: **a** schematic structure of the furnace, **b** the structure of the crucible
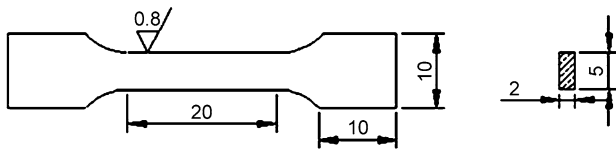
Fig. 2 Specimen for tensile tests used in this study (unit in mm)
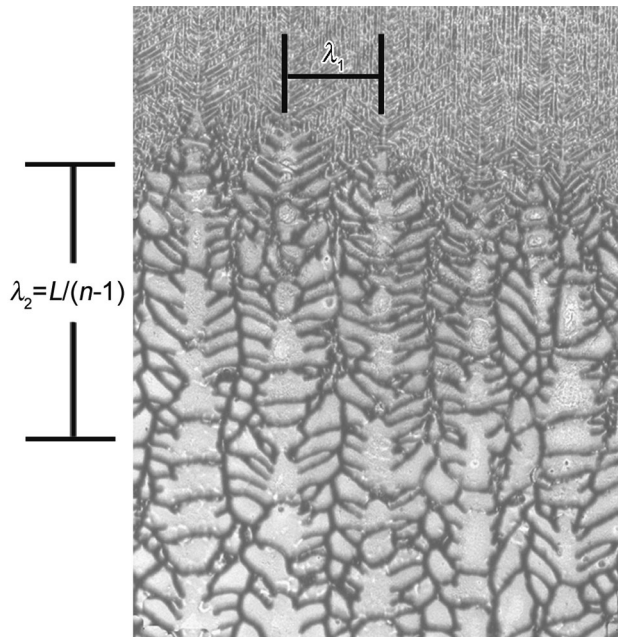
Fig. 3 Measurements of λ_1 and λ_2 on the longitudinal section

value reported here was the average value of 20–30 measurements.

3 Results and Discussion

3.1 Primary and Secondary Dendrites

Figure 4 shows OM microstructures of longitudinal and transversal section of the experimental alloy quenched during directional solidification under the temperature gradient G of 40 K/mm and the growth rates v of 10, 40, and 100 μm/s, respectively. It is seen that α(Mg) phase presents dendrite morphology along longitudinal section and typical six petaloid morphology on the transversal section. With the increase of the growth rate, both λ_1 and λ_2 become smaller and more developed corresponding to a higher cooling rate.

It is well known that both λ_1 and λ_2 have significant effects on the mechanical properties [2, 3], which are mainly determined by cooling rate R. Lots of theoretical models [11–14] were developed to evaluate λ_1 and λ_2 at various directional solidification rates, but most of them are in similar format as follows:

$$\lambda_1 = k_1 v^{-a}, \tag{1a}$$

$$\lambda_2 = k_2 v^{-b}, \tag{1b}$$

where k_1 and k_2 are the material-dependent coefficients related to alloy composition, liquidus slope, and distribution coefficient, and a and b are called the growth rate
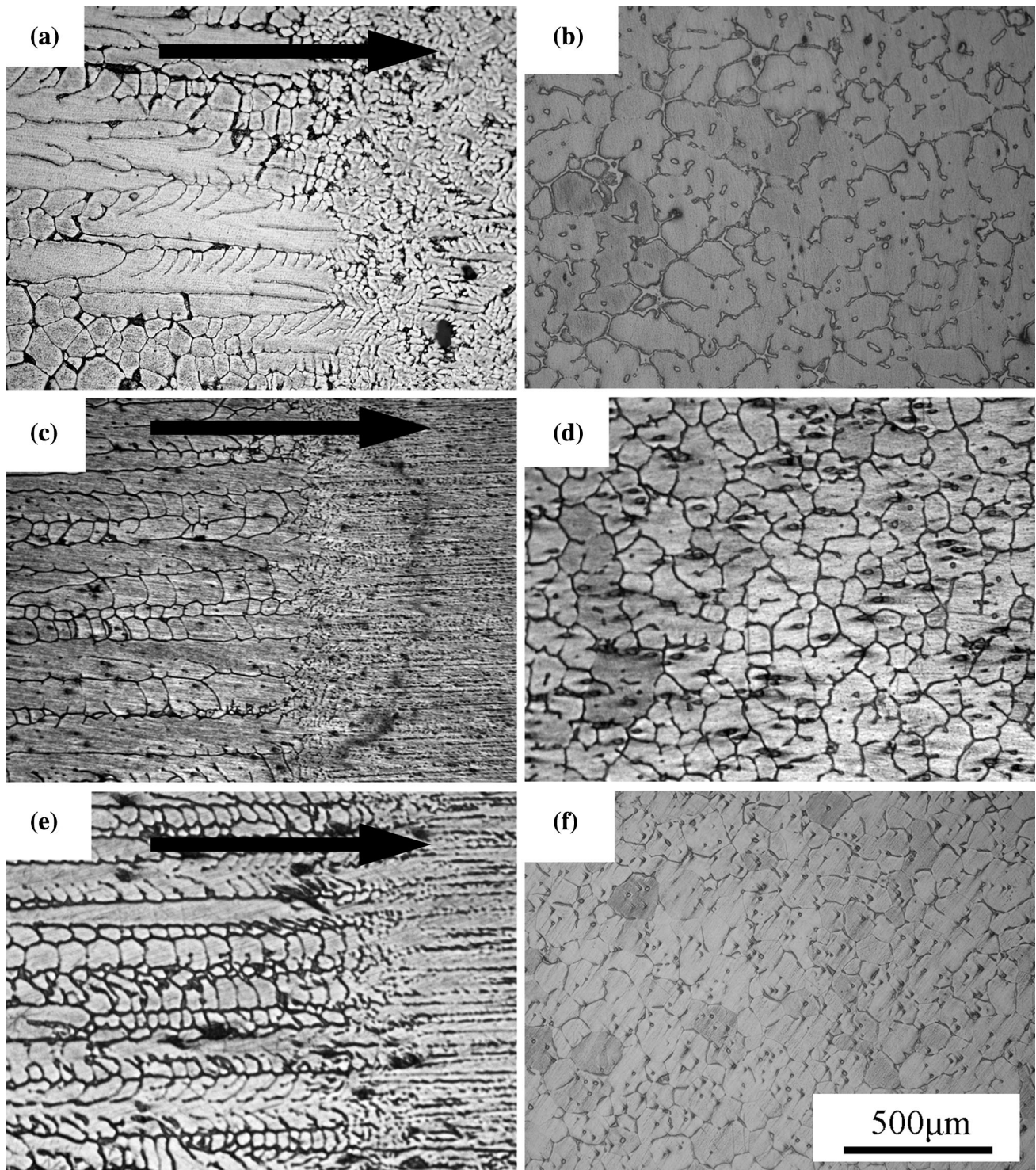
Fig. 4 OM microstructures of the directionally solidified Mg–2.49Nd–1.82Gd alloy under the temperature gradient of 40 K/mm at the growth rates of 10 μm/s **a**, **b**, 40 μm/s **c**, **d**, and 100 μm/s **e**, **f**, respectively (**a**, **c**, **e** longitudinal sections; **b**, **d**, **f** transverse sections)

exponents related to undercooling and temperature gradient during solidification.

Meanwhile, the cooling rate R can be calculated from v by multiplying G [1],

$$R = G \times v. \tag{2}$$

Thus, Eq. (1a, b) can be modified as follows for directional solidified samples,

(a)

(b)
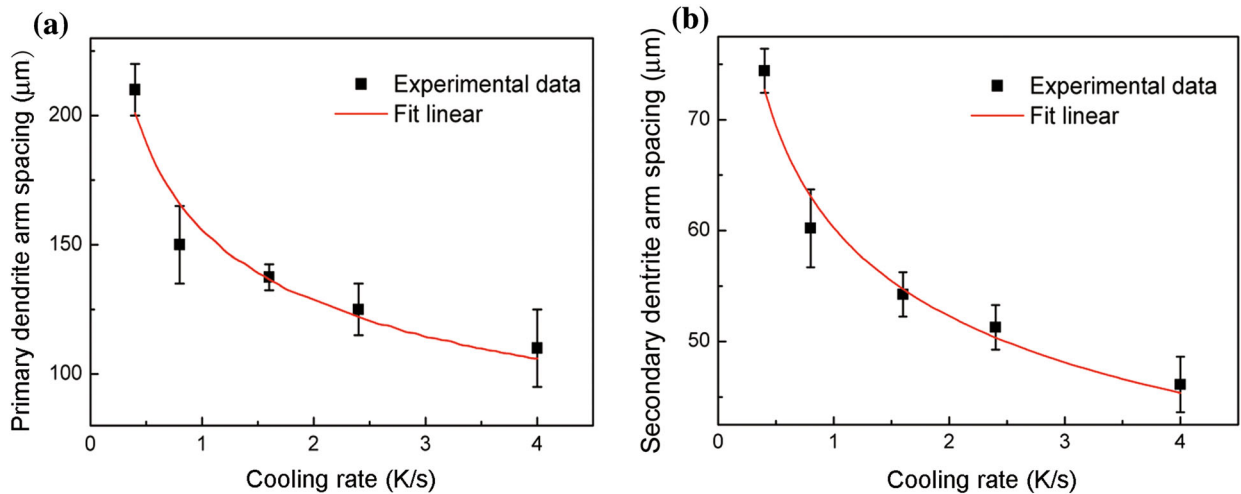
Fig. 5 Variation of the primary dendrite arm spacing λ_1 **a** and the secondary dendrite arm spacing λ_2 **b** with the cooling rate R for Mg–2.49Nd–1.82Gd alloy under $G = 40$ K/mm

$$\lambda_1 = k_1 (R/G)^{-a}, \tag{3a}$$

$$\lambda_2 = k_2 (R/G)^{-b}, \tag{3b}$$

Figure 5 shows the variations of λ_1 and λ_2 with different cooling rates R. Through linear regression analysis, λ_1 and λ_2 can be described at the temperature gradient G of 40 K/mm as follows:

$$\lambda_1 = 8.0415 \times 10^{-6} R^{-0.279}, \tag{4a}$$

$$\lambda_2 = 6.8883 \times 10^{-6} R^{-0.205}, \tag{4b}$$

where R is in K/s, λ_1 and λ_2 in m.

According to theoretical models [11–14], λ_1 was proportional to $v^{-1/4}$ and λ_2 proportional to $v^{-1/3}$. When G was constant, λ_1 should be proportional to $R^{-1/4}$ and λ_2 should be proportional to $R^{-1/3}$. Our experimental results of the cooling rate exponent value of λ_1 are slightly higher than that of the theoretical model, while the cooling rate exponent value of λ_2 is lower than the theoretical values. The reasons for the deviation may be as follows: (1) The theoretical models are proposed for binary alloy and developed on some assumption, such as non-interaction between alloying elements, which are not true for ternary alloy, (2) Some experimental errors, such as solidification parameter errors and spacing measurement errors, may also cause the deviation of experimental results from ideally designed values. However, the results are close to the theoretical predications.

### 3.2 Interdendritic Phases

Figure 6 shows XRD analysis results of the experimental alloy prepared by directional solidification with the various growth rates at the fixed temperature gradient 40 K/mm,
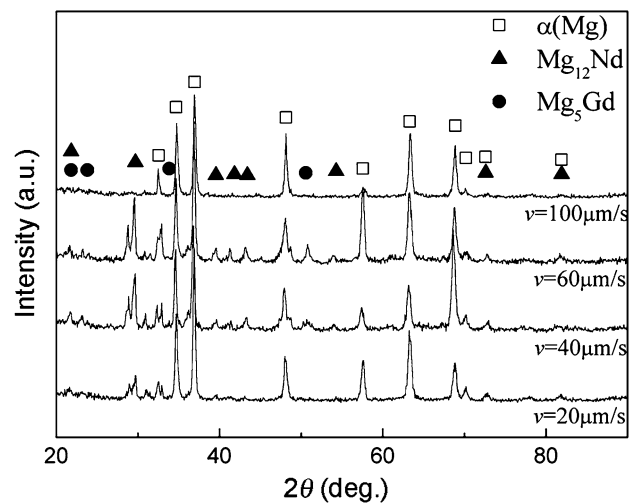
Fig. 6 XRD analysis results of Mg–2.49Nd–1.82Gd alloys

and only α(Mg), $Mg_{12}Nd$, and Mg_5Gd phases have been detected. SEM microstructures of the experimental alloy at the growth rates of 10, 40, and 100 μm/s are given in Fig. 7. It is seen that the interdendritic phase can be classified into two types, one with white rectangular-like shape marked as A and the other with a gray lamellar morphology marked as B in Fig. 7b, d, and f, which was further analyzed by selected area electron diffraction (SAED) as shown in Fig. 8. It is confirmed that the white phase A is Mg_5Gd with face centered cubic (FCC) crystalline structure, and the gray phase B is $Mg_{12}Nd$ with tI26 crystalline structure. The orientation relationship between $Mg_{12}Nd$ phase and the matrix is identified to be $[01\bar{1}2]_\alpha // [137]_{Mg_{12}Nd}$.

S. Liu *et al.*: Acta Metall. Sin. (Engl. Lett.), 2014, **27**(6), 1134–1143
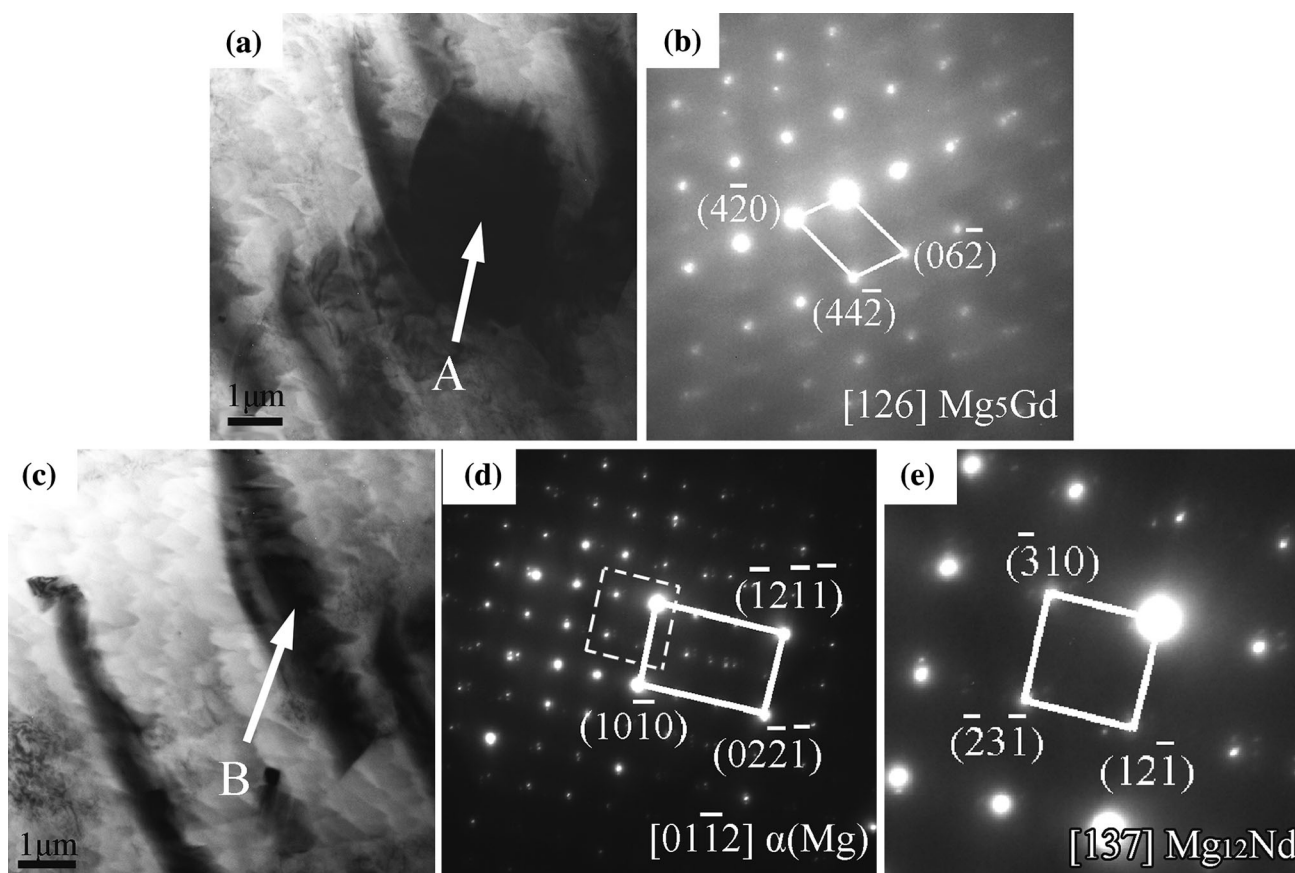
1139
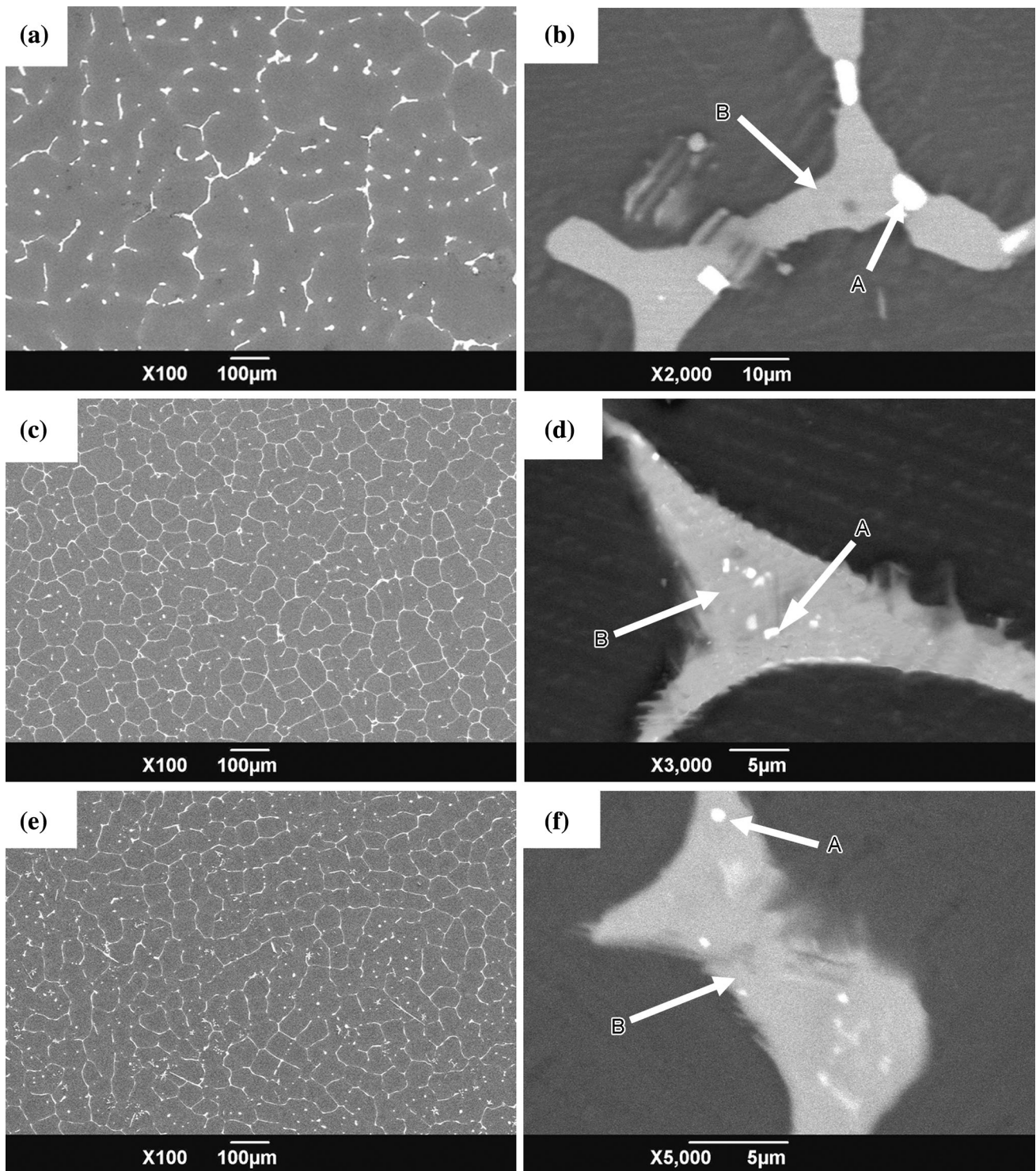
Fig. 7 SEM microstructures of transversal section and phase identification results of directional solidified Mg–2.49Nd–1.82Gd alloys under constant temperature gradient 40 K/mm at different growth rates: **a**, **b** 10 μm/s; **c**, **d** 40 μm/s; **e**, **f** 100 μm/s

It should be pointed out that $Mg_{12}Nd$ phase dissolves up to 5.47 wt% Gd according to EDS analysis. Earlier research [15, 16] showed that $Mg_{12}(Nd, Gd)$ phase is associated with improved mechanical properties, and the creep properties of Mg–Nd–Gd alloys during high-temperature exposure compared to $Mg_{12}Nd$ phase were formed in Mg–Nd-based alloy, because dissolution of a certain amount of Gd in $Mg_{12}Nd$ phase could arouse lattice

Fig. 8 Transversal section TEM microstructures and SAED patterns of directional solidified Mg–2.49Nd–1.82Gd alloys under constant temperature gradient 40 K/mm at the growth rate 40 μm/s: **a** TEM-BF image, **b** SAED of the phase A, **c** TEM-BF image, **d** SAED of the phase B, **e** local enlarger of SAED boxed by *dash line* in **d**

distortion and enhance the performance of $Mg_{12}Nd$ compound.
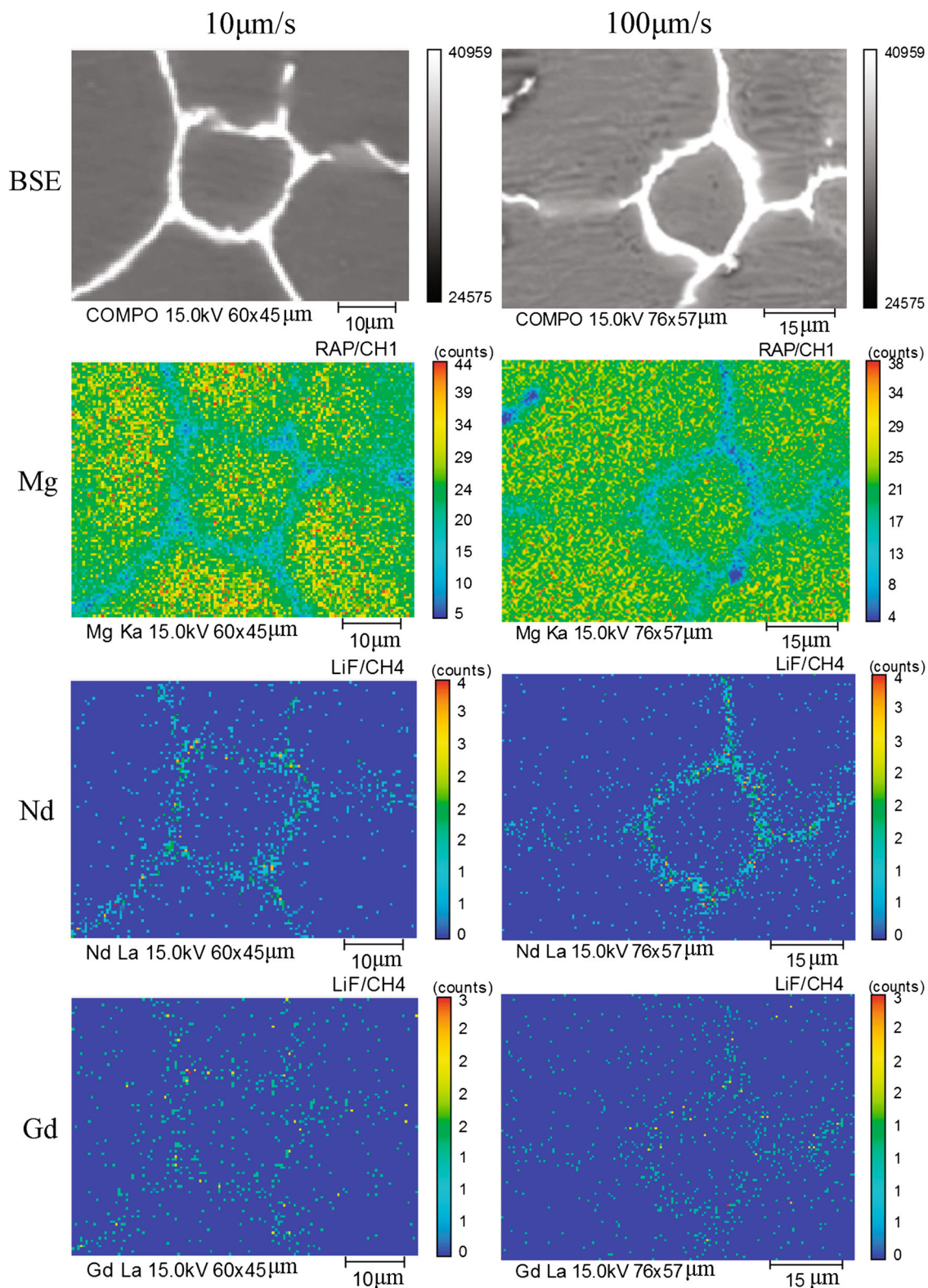
3.3 Microsegregation

Microsegregation is another important factor determining the mechanical properties because it can lead to the increase of non-equilibrium phases in solidification structure [17]. Figure 9 shows BSE image and EMPA maps of Mg, Nd, and Gd in the experimental samples prepared with the growth rates of 10 and 100 μm/s. As expected, Nd and Gd mainly distributes on the grain boundaries. Figure 10 shows the measured concentration profiles of the elements Nd and Gd as a function of the solid fraction at the growth rates of 10 and 100 μm/s, respectively. Both Nd and Gd concentrations within α(Mg) matrix increase gradually as the solidification progresses until the formation of eutectic near the end of solidification, where abrupt increase in Nd and Gd concentrations is observed.

This is mainly because the solubility of Nd and Gd is different in the liquid and solid phases [18]. For the experimental alloy with the value of solute redistribution coefficient being less than one, the solutes, such as Nd and Gd, rejected from the solid–liquid interface and developed a solute-rich region in the liquid in front of the solidification interface. With the development of solidification process, the concentration of the solutes increased in the remaining liquid. Finally, the interdendritic compounds, such as $Mg_{12}Nd$ or Mg_5Gd, were formed, when the concentration of solute-rich region reached eutectic composition. As a result, the solute content was low in the first formed α(Mg) and then further increases with development of solidification process.

It is also noted from Fig. 10 that microsegregation of Gd depends more on the growth rate in the final microsegregation, compared with Nd. This is likely due to the large back diffusion of Gd in α(Mg), which makes less Gd in the remaining liquid with higher growth rate. The concentration profiles of the elements Nd and Gd calculated by Scheil model coupled with Thermo-Calc software [19] are also given in Fig. 10. It is seen that there are appreciable discrepancies between the experimental results and the calculated ones, which is mainly due to the back diffusion within α(Mg) matrix, being unconsidered in Scheil model.
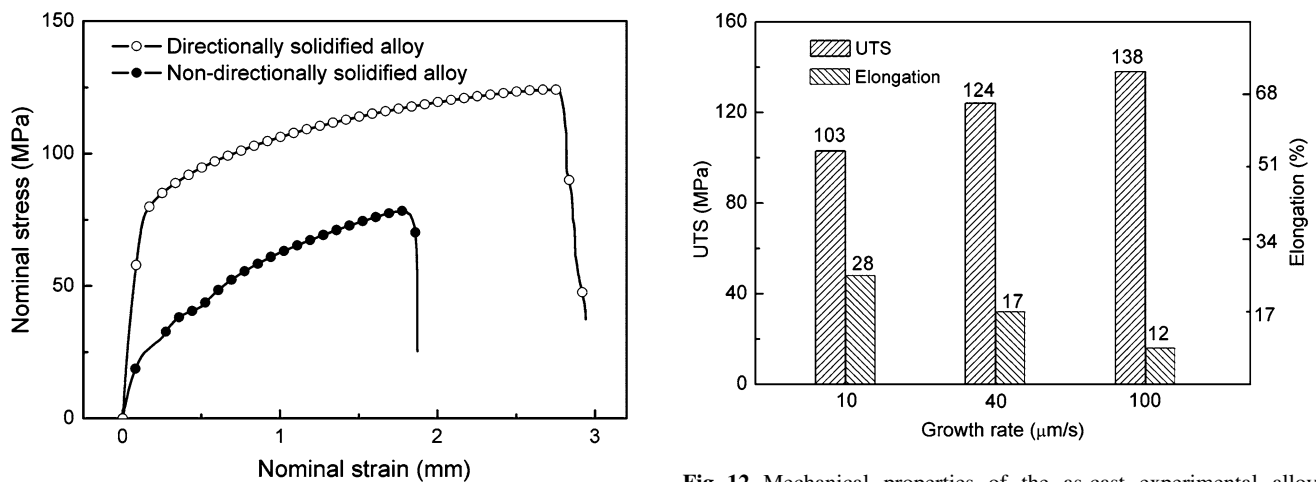
Fig. 9 EPMA backscatter images and Mg, Nd, and Gd element distribution maps of Mg–2.49Nd–1.82Gd alloy after directional solidification under the growth rate of 10 and 100 μm/s at $G = 40$ K/mm

(a)

(b)
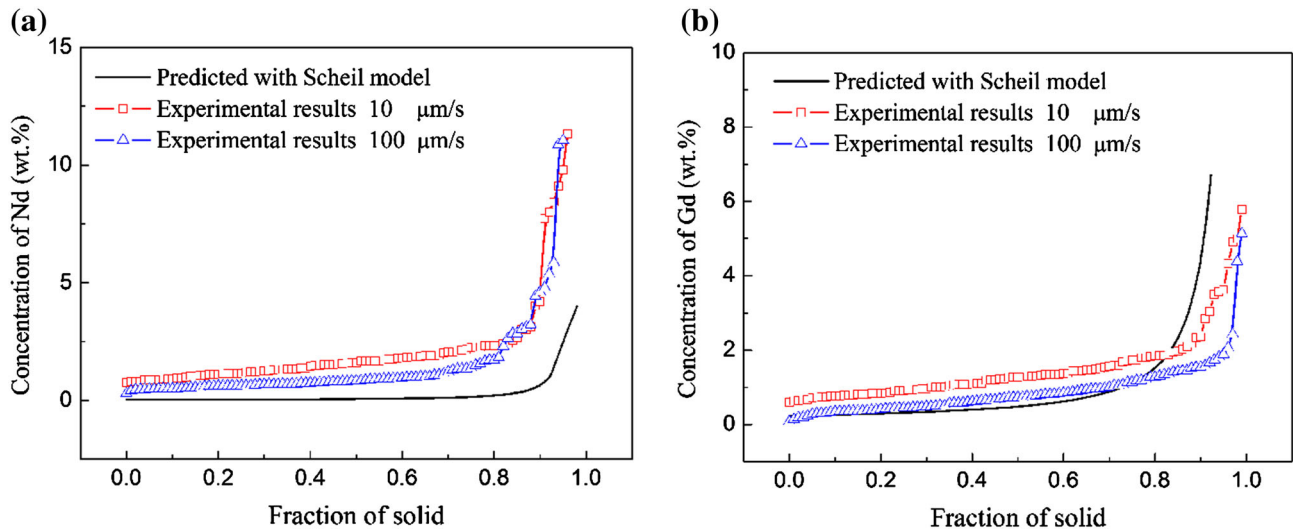
Fig. 10 Microsegregation of alloying elements in Mg–2.49Nd–1.82Gd alloy: **a** element Nd, **b** element Gd

Fig. 11 The nominal stress–nominal strain curves for the directionally solidified and non-directionally solidified experimental alloy under the same cooling rate of 1.6 K/s

Fig. 12 Mechanical properties of the as-cast experimental alloy under the temperature gradient of 40 K/mm at the growth rate of 10, 40, and 100 μm/s, respectively

3.4 Mechanical Properties

The nominal stress–nominal strain curves for the directionally solidified and non-directionally solidified experimental alloy under the same cooling rate of 1.6 K/s are shown in Fig. 11. The ultimate tensile strength (UTS) and elongation to failure were 124 MPa and 17% for the directionally solidified alloy and 78 MPa and 8% for the non-directionally solidified alloy, respectively. The directionally solidified alloy exhibited 59% higher in ultimate tensile strength (UTS) and 112% higher in elongation than the non-directionally solidified alloy. Clearly, the directional solidification technology can improve the mechanical properties of the experimental alloy significantly. This

is because the directional solidification technology realized sequence solidification in whole casting process, which decreases the amount of solidification defects, such as shrinkage porosity and shrinkage cavity.

A comparison of the mechanical properties of the as-cast experimental alloys after directional solidification under the growth rates of 10, 40, and 100 μm/s at $G = 40$ K/mm has also been done subsequently, shown in Fig. 12. It is showed that the variation of the growth rate has a significant impact on the mechanical properties of the experimental alloy. The tensile strength is improved from 103 MPa with the growth rate of 10 μm/s to 138 MPa with the growth rate of 100 μm/s. The strength of the experimental alloy increases by 34%, and the corresponding elongation decreases by 57%.

The main reason for the improvement of the tensile strength and reduction of elongation is the finer microstructure and the smaller size of the second phase due to the increase of growth rate (cooling rate). It can be seen from Fig. 5, both λ_1 and λ_2 become smaller with the increase of the cooling rate, and based on the Hall–Petch relationship, the strength of the experimental alloy would be improved [20]. Meanwhile, the average size and the volume fraction of interdendritic decreases with the increase of the cooling rate, thus the crack source should be reduced on some extent [2, 3]. Furthermore, $Mg_{12}(Nd, Gd)$ compounds contained a certain amount of Gd, which could arouse lattice distortion and enhance the performance of $Mg_{12}(Nd, Gd)$ compounds [15, 16]. Otherwise, a certain amount of Nd and Gd dissolved in $\alpha(Mg)$, which would improve the mechanical properties of $\alpha(Mg)$ matrix.

4 Conclusions

(1) The directionally solidified Mg–3.0Nd–1.5Gd alloy is mainly consisted of $\alpha(Mg)$ dendrite, interdendritic $\alpha(Mg) + Mg_{12}(Nd, Gd)$ eutectic, and Mg_5Gd phase.

(2) $\alpha(Mg)$ primary dendrite arm spacing λ_1 and the secondary dendrite arm spacing λ_2 are depended on the cooling rate R in the form $\lambda_1 = 8.0415 \times 10^{-6} R^{-0.279}$ and $\lambda_2 = 6.8883 \times 10^{-6} R^{-0.205}$ under a constant temperature gradient G of 40 K/mm at the cooling rates R between 0.4 and 4 K/s.

(3) There are significant discrepancies for the solute profiles of elements Nd and Gd between the calculated results using Scheil model and the experimental ones determined by EPMA because of back diffusion of alloying elements within $\alpha(Mg)$ matrix, being unconsidered in Scheil model. And microsegregation of Gd depends more on the growth rate, compared with Nd.

(4) The directionally solidified experimental alloy exhibits higher strength than the non-directionally solidified alloy. And the tensile strength of the directionally solidified experimental alloy is improved, while the corresponding elongation decreases with the increase of the growth rate.

References

[1] H.Z. Fu, J.J. Guo, L. Liu, J.S. Li, *Directional Solidification and Processing of Advanced Materials* (Science Press, Beijing, 2008), p. 237

[2] C. Zhang, D. Ma, K.S. Wu, H.B. Cao, G.P. Cao, S. Kou, Y.A. Chang, X.Y. Yan, Intermetallics **15**, 1395 (2007)

[3] X.W. Zheng, A.A. Luo, C. Zhang, J. Dong, R.A. Waldo, Metall. Mater. Trans. A **43**, 3239 (2012)

[4] D. Mirkovic, R. Schmid-Fetzer, Metall. Mater. Trans. A **40**, 958 (2009)

[5] J.L. Li, R.S. Chen, Y.Q. Ma, W. Ke, Acta Metall. Sin. (Engl. Lett.) **26**, 728 (2013)

[6] Z. Yang, J.P. Li, J.X. Zhang, G.W. Lorimer, J. Robson, Acta Metall. Sin. (Engl. Lett.) **21**, 313 (2008)

[7] F. Czerwinski, *Magnesium Alloys—Design, Processing and Properties* (InTech, Rijeka, 2011), p. 13

[8] Y. Negishi, T. Nishimura, M. Kiryuu, S. Kamado, Y. Kojima, R. Ninomiya, J. Jpn. Inst. Light Met. **45**, 57 (1995)

[9] A. Bell, V. Srivastava, G.W. Greenwood, H. Jones, Z. Metall. **95**, 369 (2004)

[10] J.H. Li, Rare Met Mater. Eng. **39**(1), 101 (2010) (in Chinese)

[11] J.D. Hunt, *Solidification and Casting of Metals* (The Metal Society, London, 1979), p. 3

[12] W. Kurz, D.J. Fisher, Acta Metall. **29**, 11 (1981)

[13] T.Z. Kattamis, M.C. Flemings, Trans. TMS-AIME **233**, 992 (1965)

[14] J.D. Hunt, S.Z. Lu, Metall. Trans. A **27**, 611 (1996)

[15] Q.M. Peng, J.L. Wang, Y.M. Wu, L.M. Wang, Mater. Sci. Eng. A **433**, 133 (2006)

[16] J.H. Li, G. Sha, T.Y. Wang, W.Q. Jie, S.P. Ringer, Mater. Sci. Eng. A **534**, 1 (2012)

[17] S.C. Michelic, J.M. Thuswaldner, C. Bernhard, Acta Mater. **58**, 2738 (2010)

[18] R.T. Jessica, D.S. Nicholas, J.W. Jones, T.M. Pollck, Metall. Mater. Trans. A **41**, 2435 (2010)

[19] J.O. Andersson, T. Helander, L. Höglund, P.F. Shi, B. Sundman, Calphad **26**, 273 (2002)

[20] J.H. He, X.Y. Tang, N.P. Chen, Acta Metall. Sin. (Engl. Lett.), **4**, 21 (1991)